Journal of Catalysis 258 (2008) 228–234

Contents lists available at ScienceDirect

Journal of Catalysis

www.elsevier.com/locate/jcat

Investigation on the mechanism of diffusion in mesopore structured ZSM-5 and improved heavy oil conversion

Liang Zhao, Baojian Shen *, Jinsen Gao, Chunming Xu *

State Key Laboratory of Heavy Oil Processing; the Key Laboratory of Catalysis of CNPC; and Faculty of Chemical Science and Engineering, China University of Petroleum, Beijing Changping, 102249, China

ARTICLE INFO

Article history:
Received 19 February 2008
Revised 13 June 2008
Accepted 15 June 2008
Available online 16 July 2008

Keywords:
Mesopore ZSM-5
Diffusion
Phase transition
Re-arrangement
Adsorption heat
Activation energy
Heavy oil cracking

ABSTRACT

A large probe molecule, cumene, was chosen to study diffusion and adsorption on mesopore structured ZSM-5, using a high precision intelligent gravimetric analyzer. Compared with ZSM-5, a 2–3 order of magnitude increase in the diffusion coefficient of cumene was observed on the mesopore structured ZSM-5. The increased adsorption rate and the increased adsorption heat with increased cumene coverage, supported a mechanism of diffusion, phase transition, and re-arrangement of cumene molecules during the adsorption process on the mesopore structured ZSM-5. The introduced mesopores also decreased the diffusion–adsorption activation energy by a factor of 4.6. Consequently, although the amount of strong Brønsted acid sites decreased, the conversion of cumene on the mesopore structured ZSM-5 catalyst doubled compared to ZSM-5 catalyst, and the total light olefins yield increased by 2.47 wt% with Daqing heavy oil as a feedstock.

1. Introduction

ZSM-5 zeolites have been widely used as catalysts and selective sorbents in the petrochemical industry owing to their high thermal stability, intrinsic acidity, high surface area and well-defined porosity. One of the most recent developments is the use of ZSM-5 in the conversion of heavy oil to light olefins [1,2]. The uniform micropore distribution of zeolites is responsible for their high shape selectivity observed in various reactions. However, this feature also leads to diffusion limitations when large molecules diffuse in relatively narrow channels. Some active sites are hindered from contacting reactants due to restricted transport processes [3,4]. As a consequence, it is highly needed to develop new materials with a hierarchical architecture of porosity [5–8]. Several potential solutions have been proposed to overcome the diffusion limitation imposed by zeolitic structures: synthesizing new zeolites with larger pores, such as ITQ-21 [9]; synthesizing meso–micropore, micro–micropore composite zeolite, such as Y/MCM-41 [10], ZSM-5/MCM-41 [11,12], MAS-5 [13], ZSM-5/Y [14]; preparing smaller zeolite particles [15,16] and modifying the pore structure of zeolites [17–19]. Among these, an innovative post-treatment method, desilication, has attracted extensive attention due to the creation of a network of micropores and mesopores [20–24].

The diffusion capability of large molecules in zeolite channels can be improved by the introduction of mesoporosity, which has been indirectly proven by enhanced catalytic performance with model compounds. Ogura et al. [20] performed catalytic cracking of cumene and the results showed that the micro-mesoporous ZSM-5 exhibited almost twice the conversion of microporous ZSM-5. Su et al. [24] reported that Mo-modified catalyst on mesoporous HZSM-5 zeolite showed a very high catalytic performance in the conversion of methane to aromatics when compared with conventional Mo/HZSM-5 catalyst.

Recently, Groen et al. [25] reported pioneering work in which they provided direct experimental evidence supporting improved diffusion in mesoporous ZSM-5 zeolite. The Tapered Element Oscillating Microbalance technique was employed and the diffusion capability of calcined and alkaline-treated ZSM-5 zeolite was studied, using neopentane as a probe molecule. The results show that the amount of equilibrium adsorption in alkaline-treated zeolite is ca. 15% lower than that in calcined zeolite, and this was ascribed to the lower micropore volume of the former. Although the uptake rate of neopentane in the calcined zeolite is extremely slow, the uptake rate in alkaline-treated zeolite is greatly enhanced by the network of mesopores. They concluded that the characteristic diffusion path length in the mesoporous crystals is dramatically reduced, but the diffusivity in both zeolite systems was the same.

However, the diffusion mechanism of large probe molecules is not well understood and whether or not increasing the diffusion rate of such molecules results in increased catalytic conversion has

* Corresponding authors. Faxes: +86 10 89733369 (B. Shen), +86 10 89733392 (C. Xu).
E-mail addresses: baojian@cup.edu.cn (B. Shen), xcm@cup.edu.cn (C. Xu).

0021-9517/$ – see front matter
doi:10.1016/j.jcat.2008.06.015

not been established. Furthermore, dynamic and thermodynamic data, such as the activation energy and adsorption heat, are not available for ZSM-5. Such data are helpful in understanding the diffusion process and the catalytic performance. However, until now there is still a research gap in this important area, which needs attention.

In the present work, the diffusion mechanism, the adsorption dynamics and the thermodynamic properties of the diffusion of the probe molecule cumene in ZSM-5 with different pore size distributions has been studied using a high precision intelligent gravimetric analyzer (IGA). The catalytic performance of the prepared zeolites for cumene and Daqing heavy oil cracking are also reported.

2. Experimental

2.1. Preparation of the samples

A commercially available NaZSM-5 zeolite (which was manufactured by the seeding method of hydrothermal synthesis) was used as standard material, and the ion exchanged H form of ZSM-5 was designated as "OZ5" in this work. NaZSM-5 zeolites were alkali-treated under different conditions as listed in Table 1 (designated as "AZ5"). First, 5.0 g NaZSM-5 zeolite was added to an aqueous NaOH solution (100 ml) and stirred at constant temperature. After a certain period of alkali treatment, the slurry was cooled rapidly to room temperature in an ice bath, filtered and washed with distilled water until a neutral pH of filtrate was obtained. The remaining solid was then dried in air at 393 K for 4 h.

After drying, the alkali-treated NaZSM-5 was ion exchanged with 0.4 M $(NH_4)_2SO_4$ aqueous solution and stirred at 363 K for 60 min, followed by filtering and rinsing with distilled water to remove sodium ions. This procedure was repeated twice to obtain NH_4ZSM-5. After drying at 393 K overnight, the NH_4ZSM-5 was then calcined in static air at 813 K for 4 h to form the HZSM-5 samples designated by AZ5-1, AZ5-2 and AZ5-3.

2.2. Characterization

X-ray diffraction patterns were measured using a Shimadzu-6000 diffractometer with Cu$K\alpha$ radiation at 40 mA and 40 mV. The scan rate was 4° per min for the range of 5 to 50° to confirm the structure of ZSM-5 and 0.5° per min for the range of 22.5 to 25° to identify characteristic peaks of the ZSM-5 zeolite.

The SiO_2/Al_2O_3 molar ratios of ZSM-5 zeolites were measured on a ZSX 100 e X-ray fluorescent analyzer.

N_2-adsorption/desorption isotherms were recorded on a Quantachrome Autosorb Automated Gas Sorption analyzer at 77 K. The total surface area was calculated according to the BET isothermal equation, and the micropore volume, the mesopore volume, and external surface area were evaluated by the t-plot method. The pore size was reported as the average pore diameter.

The measurement of cumene diffusion in ZSM-5 zeolites was done using a computer-controlled intelligent gravimetric analyzer (IGA, Hiden Analytical Ltd., Warrington, UK). A sensitive microbalance (resolution of 0.1 μg) was mounted in a thermostated enclosure to remove thermal coefficients of the weighing system and thus provide high stability and accuracy. The sample was degassed under a vacuum of less than 10^{-3} Pa at 773 K for 10 h prior to the adsorption measurement. The sample temperature was regulated within 0.1 K by either a water bath or a furnace. The pressure was determined using two high accuracy Baratron pressure transducers and increased gradually to obtain the entire equilibrium adsorption isotherm. For each step, the amount of sorbate introduced in the system was kept small enough to keep the adsorption process isothermal. The increases of weight were continuously recorded.

Table 1
Conditions of alkali-treatment and SiO_2/Al_2O_3 ratio after alkali-treatment of ZSM-5 zeolite

Sample	SiO_2/Al_2O_3 molar ratio	Treatment time (min)	Temperature of water bath (K)	Concentration of NaOH solution (mol/L)
OZ5	30	–	–	–
AZ5-1	29	120	333	0.25
AZ5-2	24	300	353	0.20
AZ5-3	22	300	343	0.25

The IR spectroscopic (BIO-RAD FTS3000) self-supporting wafer technique was used to determine the acidic properties of the zeolites. The wafers (10–20 mg on 1.54 cm^2) were prepared from powdered zeolites and placed into a sample holder of an in situ IR cell. Initially, the samples were heated and dried in vacuum at 623 K for 1 h. The sample was then cooled to room temperature. The acidity of the zeolite was determined by pyridine vapor, which was introduced into the IR cell at room temperature for 15 min at 2.67 Pa. The sample was heated to 473 K and desorbed in vacuum for 10–20 min at this temperature. Subsequently, the sample was cooled to room temperature. Similarly, the sample was then heated to 623 K and desorbed in vacuum for 10–20 min and cooled to room temperature.

2.3. Catalyst preparation and catalytic reactions

The catalysts for cumene cracking were prepared by pressing the proton form of AZ5 or OZ5 samples into pellets followed by crushing, and sieving to obtain 40–60 mesh zeolite particles. The catalysts were deactivated by 100% steam at 1023 K for 6 h. A mixture of 35 wt% zeolite particles and 65 wt% quartz sand were used in the catalyst activity tests.

The catalysts for heavy oil cracking were prepared from 30 wt% phosphorus modified zeolite, 51 wt% kaolin, and 19 wt% alumina binder (dry basis of Al_2O_3). They were mechanically mixed to form a homogeneous slurry. The slurry was dried at 393 K for 4 h and calcined at 813 K for 4 h. The obtained solids were crushed to particles 40–60 mesh that were subsequently deactivated by 100% steam at 1023 K for 6 h. Incipient wetness impregnation was used to modify the zeolite by adding $(NH_4)_2HPO_4$ aqueous solution. The impregnated zeolite was dried at 393 K overnight and then calcined at 813 K for 4 h. The content of phosphorus in the zeolite was 5 wt% of P_2O_5.

Cumene (A.R.) was employed as the model compound to test the catalytic performance of the zeolites. A standard micro-activity test (MAT) unit designed in accordance with ASTM D-3907 was used as the reactor. The reactions were carried out at 898 K and the feed injection time was 60 s. The catalyst to oil ratio was 3, and the amount of catalyst was 3.0 g. After reaction, catalyst stripping was carried out for 5 min using a N_2 flow of 30 cm^3/min. During the reaction and stripping steps, the liquid products were collected in the corresponding glass receivers and the gaseous products were collected in a gas burette by water displacement.

Daqing heavy oil was also employed as the feedstock for catalytic pyrolysis testing. The properties of the feedstock are shown in Table 2. The catalytic pyrolysis test was performed in a standard confined fluidized bed reactor system. The reactions were carried out at 933 K and the feed injection time was 36 s. The ratio of catalyst to oil was 16 (wt/wt), the ratio of water to oil was 0.6 (wt/wt), and the amount of catalyst loaded was 50 g.

The catalytic cracking reaction product consisted of pyrolysis gas, liquid, and coke. An Agilent 6890 gas chromatograph with ChemStation software was used to determine the volume percentages of pyrolysis gas components, which were converted to mass percentages using the ideal gas equation of state. The coke content of the catalysts was determined by a coke analyzer.

Table 2
Properties of heavy oil feedstock

Items	Daqing heavy oil
Density (g/cm^3) (293 K)	0.913
Viscosity (Pa s) (323 K)	0.213
Carbon residue (wt%)	4.3
M_n (g/mol)[a]	577
H (wt%)	12.87
C (wt%)	86.77
H/C	1.78
Saturated carbons	59.2
Aromatics	29.1
Resins and asphaltenes	11.7

[a] M_n: average molecular weight.

3. Results and discussion

3.1. Textural features of the alkali-treated ZSM-5

XRD (cf. Fig. 1) showed that the ZSM-5 crystal structure was retained after alkali-treatment and ion-exchange. The position of the diffraction peaks assigned to ZSM-5 did not change, but the intensity of most peaks increased slightly due to the removal of silicon species from the framework of ZSM-5 zeolite, without complete destruction of the crystal lattice.

The changes in SiO_2/Al_2O_3 molar ratio of ZSM-5 upon alkali-treatments were summarized in Table 1. The results clearly showed that Si species were preferentially dissolved, which resulted in a lower SiO_2/Al_2O_3 molar ratio of AZ5 zeolites. A similar trend was previously reported by Ogura et al. [20] and Suzuki and Okuhara [21].

N_2 adsorption isotherms on the OZ5 and AZ5 zeolites revealed that various hierarchical pore distributions had been formed upon alkali-treatment. The detailed porosity properties are listed in Table 3. The BET total surface area (S_{BET}), the mesopore surface area (S_{meso}), the total pore volume (V_P), the mesopore volume (V_{meso}), and average pore diameter of the AZ5 zeolites were significantly different from those of the OZ5 zeolite. Remarkably, the mesopore surface area of the AZ5-3, the mesopore volume, and the average pore diameter increased to 175 m^2/g (about 695%), 0.3 cm^3/g (about 614%), and 4.0 nm (about 82%) respectively, compared to the OZ5 zeolite. With the micropore properties preserved, the micropore surface area decreased by only about 30%. Groen et al. [26] indicated that a greatly enhanced mesopore surface area can be achieved in the Si/Al range of 25–50 (measured using ICP-OES on a Perkin–Elmer Optima 4300DV spectrometer).

The N_2-adsorption isotherms and pore-size distribution curves of the OZ5 and AZ5 zeolites are shown in Fig. 2. The parent OZ5 gave a Type-I isotherm with a plateau at higher relative pressures compared to AZ5 and no distinct hysteresis loop, typical of microporous materials. From the pore-size distribution curve, a small peak appeared at about 3.5 nm and the average pore diameter was confirmed to be 2.2 nm.

Upon alkali-treatment, the zeolitic structure showed a remarkably enhanced adsorption of N_2 accompanied by a hysteresis loop, indicative of extra mesoporosity. The isotherm represents Type-IV behavior. The shape of the hysteresis loop changed with alkali-treatment conditions and implied that mesopores with various diameters were formed on the zeolite. The pore-size distributions were significantly different from OZ5. The AZ5-3 gave a single peak at about 3.8 nm and the peak intensity was about 8 times that of the OZ5. The average pore diameter was 4.0 nm. The results indicate that the alkali-treatment technique yields a zeolite with the anticipated mesopore structure.

In summary, the above investigation showed that the alkali-treatment afforded the AZ5 series zeolites with mesopore structure while preserving the MFI micropore structure. Taking these four zeolites as adsorbents, the diffusion capabilities of cumene were studied.

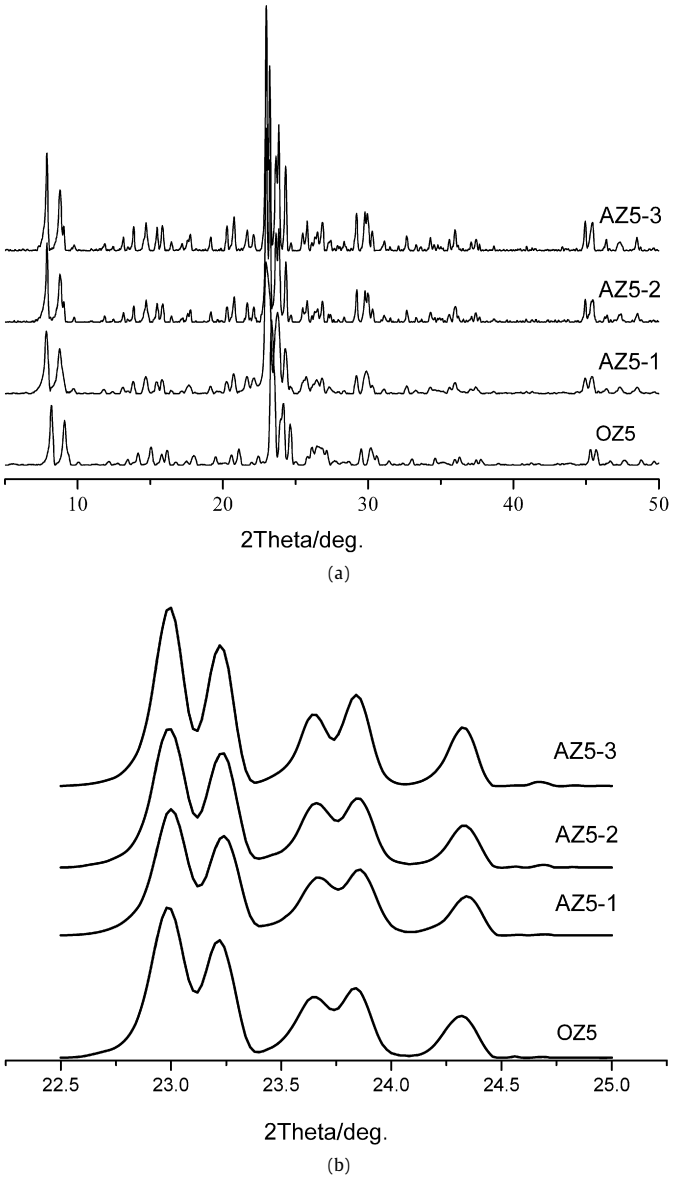

Fig. 1. XRD patterns for OZ5 and AZ5 zeolites.

Table 3
The porosity properties of the OZ5 and AZ5 zeolites

Sample	D_{aver} (nm)	S_{BET} (m^2/g)	S_{micro} (m^2/g)	S_{meso} (m^2/g)	V_p (cm^3/g)	V_{micro} (cm^3/g)	V_{meso} (cm^3/g)
OZ5	2.2	380	358	22	0.212	0.171	0.042
AZ5-1	2.4	383	347	36	0.231	0.167	0.064
AZ5-2	3.5	414	283	131	0.357	0.144	0.213
AZ5-3	4.0	427	252	175	0.431	0.130	0.300

3.2. Cumene adsorption on the OZ5 and AZ5 zeolites

The adsorption isotherms of cumene measured using the IGA instrument at 308 K on the four zeolites are presented in Fig. 3. The isotherm of OZ5 showed typical Langmuir Type-I adsorption, which reached saturation at low pressure and then increased slightly with further increase of pressure. The isotherm for AZ5-1 was similar to that of OZ5 except for a small increment in cumene uptake. However, the isotherms for AZ5-2 and AZ5-3 showed

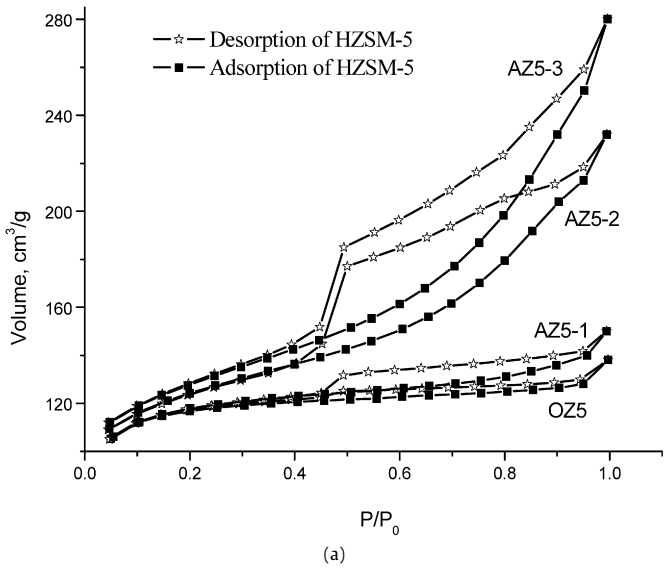

(a)

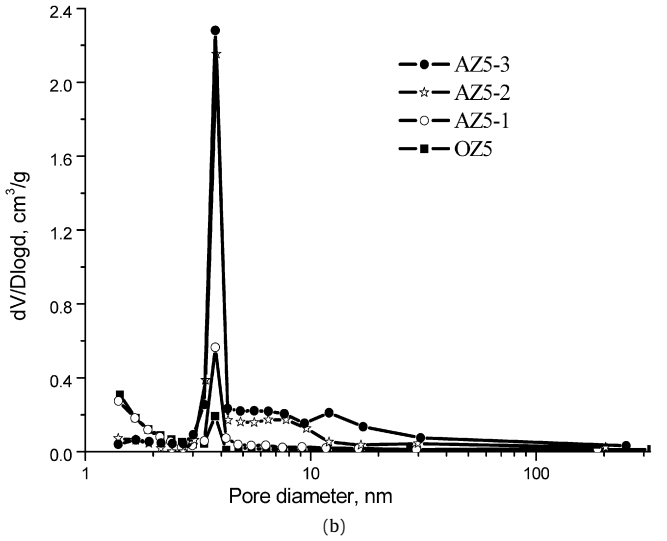

(b)

Fig. 2. (a) N_2-adsorption (■) and desorption (☆) isotherms at 77 K of OZ5 and AZ5 zeolites; (b) corresponding BJH pore-size distribution of OZ5 and AZ5 zeolites.

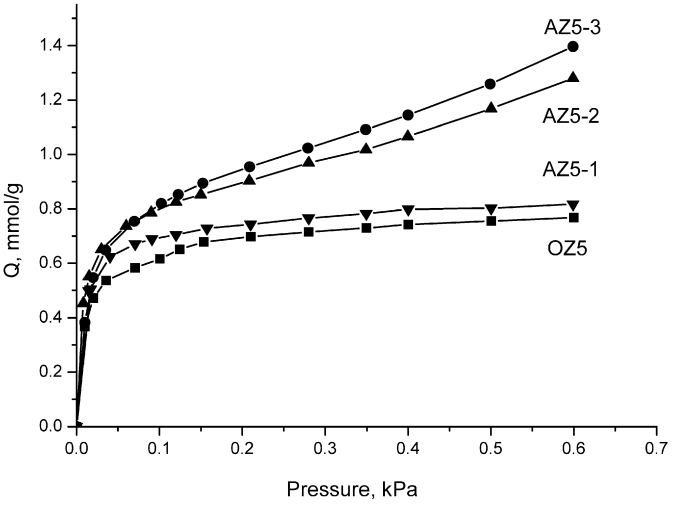

Fig. 3. The adsorption isotherms of OZ5 and AZ5 by IAG at 308 K.

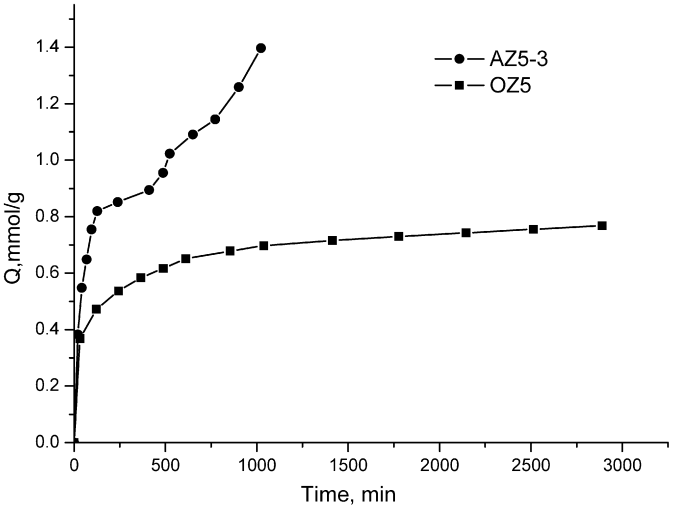

Fig. 4. The adsorption amount of cumene on OZ5 and AZ5 versus time by IGA at 308 K.

a completely different trend from the isotherms of OZ5 and AZ5-1. The AZ5-2 and AZ5-3 zeolites always exhibited higher adsorption amounts than the others over the range of test pressure, which indicates higher adsorption capacity. The adsorption amount of cumene on AZ5-2 and AZ5-3 continued to increase with pressure, especially on AZ5-3, with almost double the adsorption compared to the amount adsorbed on OZ5 at 0.6 kPa.

Comparing the adsorption phenomena of cumene on OZ5 and AZ5-3 was helpful to understand the mechanism of cumene diffusion. As shown in Fig. 4, the initial adsorption rate of cumene on OZ5 was high, and almost 48% of the maximum adsorption amount was achieved after 32 min. Then, the adsorption rate decreased, indicating that with the increase in the amount of cumene adsorbed, it becomes more difficult for cumene to diffuse into the micropore of OZ5 zeolite channels. However, it was different for AZ5-3. It seemed that there were several steps when cumene adsorbed on/into AZ5-3. At the beginning (as shown in Fig. 4), the cumene molecules adsorbed and diffused quickly on the outside surface of AZ5-3 with a high adsorption rate, this phenomenon was similar to that of OZ5. The cumene molecules also diffused easily into the mesopores and/or super-micropore of AZ5-3 at a high adsorption rate, and the amount of adsorption became higher than that on OZ5 because of the existence of mesopores (cf. Fig. 4). When sufficient cumene molecules were adsorbed on the mesopore and/or super-micropore of AZ5-3, the interaction between molecules became dominant. Consequently, a phase transition could occur, which means, the adsorption of cumene molecules changed from monolayer adsorption to multilayer adsorption or condensation. At this time, due to the "balance adsorption," the rapid decrease of adsorption rate is observed as shown in Fig. 4. After that, the cumene molecules commenced to diffuse into micropores via rearrangement. In this step the diffusion rate was low due to the limitation of pore size and interaction between molecules and zeolite walls. The increased adsorption amount can also be observed from Fig. 4 with smaller slope comparing to the very beginning. Cumene molecules could not enter the intersection of two different size pores and/or between straight channel and zig-zag channel until re-arrangement occurred. The re-arrangement of molecules resulted in an increase of adsorption amount and rate which can also be observed from Fig. 4.

It may be reasonable to understand that the combination of micropore and mesopore structure made the cumene diffusion, phase transition, and re-arrangement easier and was beneficial for an increase in adsorption capacity of a large molecule.

3.3. Diffusion coefficients of cumene on the OZ5 and AZ5 zeolites

For ZSM-5 zeolite, the diffusion in the crystals was assumed to follow Fick's law. The mathematical solution for the transient diffusion equation for a spherical particle assumes the well-known form given by Crank [27]:

$$\frac{Q_t - Q_0}{Q_\infty - Q_0} = 1 - \frac{6}{\pi^2}\sum_{n=1}^{\infty}\left[\frac{1}{n^2}\exp\left(-\frac{n^2\pi^2 t}{r_0^2}D\right)\right], \quad (1)$$

where Q_t, Q_∞ and Q_0 are the amounts adsorbed at time t, at time of sorption equilibrium and at time $t = 0$, respectively. For short time periods, Eq. (1) approaches the expression:

$$\frac{Q_t - Q_0}{Q_\infty - Q_0} = \frac{6}{r_0}\sqrt{\frac{Dt}{\pi}}. \quad (2)$$

It can be seen from Eq. (2) that the plot of $\frac{Q_t - Q_0}{Q_\infty - Q_0}$ versus the square root of time should be linear in the initial part of the curve and the slope yields the diffusion time constant D/r_0^2. This approach was mainly used in the calculation of diffusivity coefficient owing to the fact that the short time response was less susceptible to thermal effects or the distribution of adsorbent particle size.

The adsorption and desorption diffusion coefficients of cumene on the four samples at various pressures are listed in Table 4. The D_{ads} of the AZ5-3 was 1500 and 40 times more than that of the D_{ads} for cumene in OZ5 at 0.08 and 0.16 kPa, respectively. Even after a mild alkali-treatment, AZ5-1, D_{ads} was 380 and 20 times higher at 0.08 and 0.16 kPa, respectively, compared with OZ5.

The D_{des} of cumene in OZ5 was approximately equal to zero, because the change in the adsorbed amount of cumene was almost nil. The kinetic diameter of cumene is 0.68 nm, which is larger than that of ZSM-5 (0.56 nm). Consequently only small amounts of cumene can enter the pores of OZ5 through thermal motion and impinging among molecules, then adsorbing on the internal surface of the zeolite. It is difficult for cumene to diffuse out of the pores. After the introduction of mesopores into the ZSM-5 crystal, the D_{des} of AZ5-3 increased to 7.21×10^{-12} and 1.67×10^{-12} m^2/s at 0.02 and 0.08 kPa, respectively. These data indicate that the introduced mesoporosity of the zeolite significantly improved the diffusion rate. The improvement in diffusion ability is expected to greatly benefit the cracking capability of these types of large molecules.

3.4. Diffusion–adsorption activation energy of cumene on OZ5 and AZ5-3 zeolites

Cumene adsorption isotherms on OZ5 and a mesopore AZ5-3 were tested at 308, 343, 367 and 403 K. The activation energy of diffusion–adsorption was calculated by the Arrhenius equation:

$$D = A\exp\left(\frac{-E_a}{RT}\right), \quad (3)$$

wherein D, A, E_a, and T represent the diffusion/adsorption coefficient (m^2/s), pre-exponential factor, activation energy (J/mol) and temperature (K), respectively. The plot of $\ln D$ versus the T^{-1} should be linear and E_a and A can be calculated according to the slope and intercept of this line. Fig. 5 illustrates the linear relation and Table 5 lists the calculated results.

The diffusion–adsorption activation energy E_a decreased from 65 to 14 kJ/mol after mesopores were introduced in the ZSM-5 zeolite. This indicates that mesopores enhanced the diffusion rate in the zeolite but decreased the adsorption energy barrier. The decreased energy barrier will be beneficial to the transportation and cracking of reactants.

Table 4
The diffusion coefficient of cumene on four samples at 308 K

Sample	P (kPa)	$D_{ads} \times 10^{16}$ (m^2/s)	R^a	SD^b $\times 10^2$	P (kPa)	$D_{des} \times 10^{16}$ (m^2/s)	R^a	SD^b $\times 10^2$
OZ5	0.08	0.4	0.999	0.014	0.08	0	–	–
AZ5-1		164	0.997	0.175		981	0.999	0.003
AZ5-2		548	0.999	0.009		7180	0.998	0.115
AZ5-3		667	0.999	0.280		16700	0.999	0.453
OZ5	0.16	3	0.993	0.582	0.02	0	–	–
AZ5-1		71	0.998	0.001		12600	0.997	0.200
AZ5-2		77	0.999	0.001		45300	0.999	0.148
AZ5-3		122	0.996	0.096		72100	0.998	0.243

[a] R: correlation coefficient.
[b] SD: standard deviation of the fit.

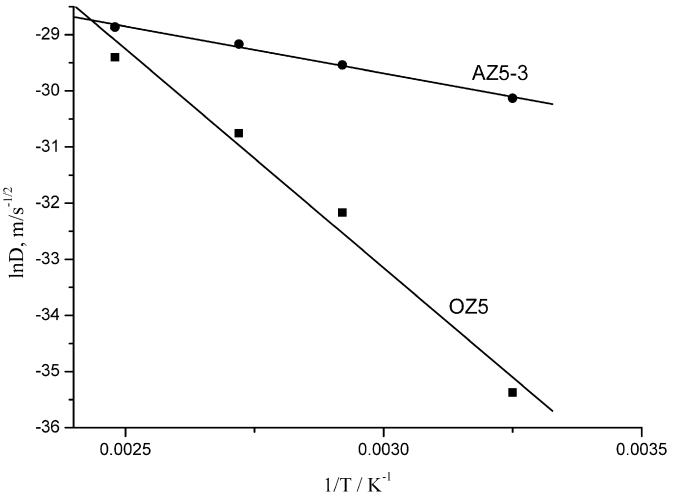

Fig. 5. Data linear fitting of the OZ5 and AZ5-3 to calculate E_a and A.

Table 5
Adsorption activation energy and pre-exponential factor of the OZ5 and AZ5-3

Sample	ln A	A	E_a (kJ/mol)	R^a
OZ5	−9.75	7.04×10^{-5}	65	0.997
AZ5-3	−24.67	1.93×10^{-11}	14	0.991

[a] R: correlation coefficient.

3.5. Heat of adsorption of cumene on the OZ5 and AZ5-3 zeolites

Thermodynamic parameters are often used to assess zeolite properties. For example, the heat of adsorption is a measure of the interaction between the zeolite/catalyst surface and the adsorbate molecules. Heat of adsorption data can describe the capacity of adsorption. Heat of sorption (Q_{st}) was estimated using the following relation:

$$\ln P = C + \frac{Q_{st}}{RT}, \quad (4)$$

wherein P, T and C respectively represent equilibrium pressure (kPa), temperature (K) and a constant.

Fig. 6 indicates that at low cumene loading the heat of cumene adsorbed on the OZ5 zeolite increased with increasing cumene coverage. Subsequently, decreased heats of adsorption were observed as the cumene coverage increased on the OZ5 zeolite. This can be explained by the fact that the heat released from different adsorption sites varies, due to the difference in the energy of the surface adsorption sites. The adsorption sites that remain vacant at a certain cumene loading have reduced energy, and therefore, the adsorption heat decreased. The interaction between adsorbate molecules and zeolite are dominant.

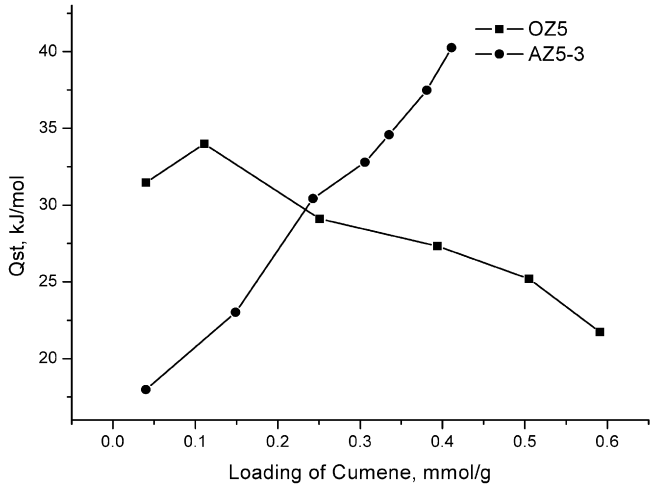

Fig. 6. The adsorption heat curve under different loading of the OZ5 and AZ5-3.

Table 6
The acidic properties of the OZ5 and AZ5-3 zeolites

Sample	473 K		623 K		473 K	623 K
	L (μmol/g)	B (μmol/g)	L (μmol/g)	B (μmol/g)	L/B	L/B
OZ5	67	584	64	560	0.11	0.11
AZ5-3	249	402	163	295	0.62	0.55

However, the adsorption heat curve of AZ5-3 increases with increasing cumene uptake. Thamm [28] and Lee and Chiang [29] have reported that the adsorption heat exhibited an unexplained increase at an intermediate loading for benzene, ethylbenzene, toluene and *p*-xylene adsorption on MFI zeolite. They suggested that this was due to a phase transition or a change in the state of the adsorbed molecules. Smit [30] focuses on the adsorption phenomenon in porous material using molecular simulation technique. They point out that phase transition is a good way to understand the inflection of adsorption isotherm and related energies changes [31,32]. In the present study, the direct experimental evidence indicated that there were several steps in the process of cumene adsorption on/into the pore system of mesopore structured ZSM-5 (AZ5-3), it may suggests that a phase transition and molecule rearrangements took place in the course of cumene diffusion. As discussed in Section 3.2 (cf. Fig. 4), a phase transition occurred in mesopores and super-micropores of zeolite because of the strong interaction between cumene molecules. However, the phase transition could not occur in micropores due to the limitation of pore volumes and molecules size. The reasonable way that cumene molecules can enter the intersection of two different size pores and/or between straight channel and zig–zag channel was a molecule re-arrangement.

Based on Fig. 4 and Fig. 6, it is likely to be concluded that the adsorption heat curves of OZ5 and AZ5-3 in Fig. 6 just reflect the initial adsorption of cumene molecules on the outside surface of OZ5, or on the outside surface and mesopore of AZ5-3.

3.6. Acidity of OZ5 and AZ5-3 zeolites

The FT-IR spectra of pyridine adsorbed on the OZ5 and AZ5-3 zeolites at 473 and 623 K were measured and Table 6 summarizes their acidic properties. From Table 6 it can be observed that an increase in the Lewis acid-sites and decrease in the Brønsted acid-sites occurred for AZ5-3 compared to OZ5. Furthermore, the total acid amount was equal, but the strong acid amount decreased. As siliceous species were selectively dissolved during alkali-treatment, the amount of residual surface Al or Si increased, and the Si to Al ratio in the framework decreased, resulting in a loss of strong Brønsted acid sites and an increase in Lewis acid sites.

Table 7
The products distribution of cumene cracking on zeolites

Catalyst	OZ5 catalyst	AZ5-3 catalyst	Arenaceous quartz
Yields of gas products (wt%)			
Methane	0.30	0.38	0.28
Ethane	0.31	0.40	0.27
Ethene	1.01	1.04	0.05
Propene	9.75	23.52	0.17
Butene	0.58	0.88	0
Yields of liquid products (wt%)			
Benzene	16.12	36.58	0.35
Toluene	0.18	0.23	0.07
Ethylbenzene	0.32	0.50	0.38
Styrene	0.40	0.46	0.77
Methyl-styrene	1.19	1.39	1.99
Propylbenzene	0.21	0.62	0.10
Cumene	69.29	33.65	95.55
Yields of solid products (wt%)			
Coke	0.34	0.36	0.03
Cumene conversion (%)	30.71	66.35	4.45

3.7. Catalytic evaluation of cumene on OZ5 and AZ5 zeolites

The cracking of cumene is a suitable model of refinery cracking because cumene cracking takes place on typical cracking catalysts and the product distribution is comparatively simple, with benzene and propene being the major products. However Corma [33] demonstrated that a total of 67 products were involved in the cumene cracking process. In our study, primary products in the gas phase were methane, ethane, ethene, propene, and butene; in the liquid phase benzene, toluene, ethylbenzene, styrene, cumene, methyl-styrene, propylbenzene and in the solid phase, coke. Among these primary products, the yields of propene and benzene dominate. The cumene cracking results are listed in Table 7.

Generally, cumene cracking occurs on Brønsted acid sites, which implies that more Brønsted acid sites will yield a higher catalytic activity. The pyridine-IR results showed that the number of Brønsted acid sites decreased after alkali-treatment, which should result in a decrease in reaction activity. However, in our studies, the cumene conversion of AZ5 is almost twice that of OZ5.

AZ5-3 has a lower diffusion–adsorption activation energy than OZ5, and this results in increased adsorption uptake. Furthermore, the larger diffusion coefficient of AZ5-3 means a faster diffusion rate which together with the increased adsorption heat, increases the turn over frequency and thus improves the conversion of cumene in the micro-mesopores ZSM-5 zeolite, even though the amount of strong Brønsted acid sites decreased compared to OZ5. Note that the conversion of cumene on arenaceous quartz, also listed in Table 7, was only 4.4 wt%, from which we can conclude that the major reaction was catalytic at this temperature.

3.8. Cracking of heavy oil

In prior studies, few researchers have used heavy oil as feed to test the activity of mesopore structured ZSM-5 catalysts, and model compounds were used instead. However the transportation of heavy oil molecules through zeolite narrow channels is limited by the large size. In order to investigate the cracking performance of heavy oil on mesopore structured ZSM-5, heavy oil was selected as feedstock and AZ5-3 catalyst (mesopore structured ZSM-5) and OZ5 catalyst (usual ZSM-5) were evaluated as shown in Table 8.

The AZ5-3 catalyst showed a 2.47 wt% increase in total olefin yield compared to that of ZSM-5, and the yield of propene on

Table 8
The products distribution of heavy oil cracking on zeolite catalysts

Catalyst	OZ5 catalyst	AZ5-3 catalyst
Yields of products (wt%)		
Dry gas	33.46	29.58
LPG	22.49	25.65
Liquid	31.93	31.58
Coke	12.12	13.19
Yields of olefins (wt%)		
Ethene	13.82	13.18
Propene	14.90	16.84
Ethene + propene	28.72	30.02
Butene	4.74	5.91
Total light olefins	33.46	35.93

AZ5-3 catalyst increased by 1.94 wt%. The results show that the mesopore structured ZSM-5 had higher cracking ability than conventional ZSM-5, because not only were transport limitations decreased by the introduced mesoporosity but more active sites were exposed to reactants. Simultaneously, the increase in yield of light olefins showed that the shape-selectivity of ZSM-5 was preserved.

4. Conclusions

The diffusion data of a large probe molecule, cumene, showed increase in both the adsorption amount and the adsorption rate on mesopore structured ZSM-5 generated by alkali-treatment, compared to untreated ZSM-5. The diffusion coefficient of cumene increased by the 2–3 orders of magnitude and the diffusion–adsorption activation energy increased by a factor of 4.6 with the introduction of mesoporous structure to ZSM-5. Both increases are ascribed to improvements in diffusion. It was found that the interaction between adsorbate molecules becomes stronger in the mesopore structured ZSM-5 during the adsorption process and this leads to a process of diffusion, phase transition, and rearrangement of cumene molecules, which increased adsorbate uptake and the heat of adsorption. As a result, the conversion of cumene on catalyst containing mesopore ZSM-5 doubled compared to the conversion on conventional ZSM-5 catalysts, and the total light olefin yield increased by 2.47 wt% when Daqing heavy oil was employed as the feedstock. The improved activity occurred despite a decrease in the strong Brønsted acid sites on the mesopore structured ZSM-5.

Acknowledgments

The authors thank professor Xuanwen Li of Peking University for fruitful discussions. Dr. Lijuan Song and Daosheng Liu at Liaoning Shihua University are acknowledged for their assistance with the IGA measurements. The authors acknowledge the supports by the National Natural Science Foundation of China through the program for Distinguished Young Scholars of China (Grant Nos. 20525621 and 20725620).

References

[1] A. Corma, F. Melo, L. Sauvanaud, F.J. Ortega, Appl. Catal. A 265 (2004) 195.
[2] X.F. Li, B.J. Shen, Q.X. Guo, J.S. Gao, Catal. Today 125 (2007) 270.
[3] A. Corma, J. Catal. 216 (2003) 298.
[4] J. Kärger, D.M. Ruthven, Diffusion in Zeolite and Other Microporous Solids, Wiley, New York, 1992, p. 14.
[5] A. Corma, Chem. Rev. 97 (1997) 2373.
[6] G. Soler-Illia, C. Sanchez, B. Lebeau, J. Patarin, Chem. Rev. 102 (2002) 4093.
[7] S. van Donk, A.H. Janssen, J.H. Bitter, K.P. de Jong, Catal. Rev. 45 (2003) 297.
[8] Y. Tao, H. Kanoh, L. Abrams, K. Kaneko, Chem. Rev. 106 (2006) 896.
[9] A. Corma, M.J. Díaz-Cabañas, J. Martínez-Triguero, F. Rey, J. Rius, Nature 418 (2002) 514.
[10] K.R. Kloetstra, H.W. Zandbergen, J.C. Jansen, H. van Bekkum, Microporous Mater. 6 (1996) 287.
[11] K.R. Kloetstra, J.C. Jansen, H. van Bekkum, Prepr. Am. Chem. Soc. Div. Pet. Chem. 41 (1996) 412.
[12] L. Huang, W. Guo, P. Deng, Z. Xue, Q.J. Li, Phys. Chem. B 104 (2000) 2817.
[13] Z. Zhang, Y. Han, L. Zhu, R. Wang, Y. Yu, S. Qiu, D. Zhao, F.S. Xiao, Angew. Chem. Int. Ed. 40 (2001) 1258.
[14] B.J. Shen, H.L. Chen, J. Guo, H.F. Pan, Bull. Chem. Soc. Jpn. 78 (2005) 2238.
[15] B.A. Holmberg, H. Wang, J.M. Norbeck, Y. Yan, Microporous Mesoporous Mater. 59 (2003) 13.
[16] C.J.C. Jacobsen, C. Madsen, T.V.W. Janssens, H.J. Jakobsen, J. Skibsted, Microporous Mesoporous Mater. 39 (2000) 393.
[17] Y. Tao, H. Kanoh, K. Kaneko, J. Am. Chem. Soc. 125 (2003) 6044.
[18] Y. Tao, H. Kanoh, K. Kaneko, J. Phys. Chem. B 107 (2003) 10974.
[19] X.T. Wei, P.G. Smirniotis, Microporous Mesoporous Mater. 97 (2006) 97.
[20] M. Ogura, S. Shinomiya, J. Tateno, Y. Nara, M. Nomura, E. Kikuchi, M. Matsukata, Appl. Catal. A 219 (2001) 33.
[21] T. Suzuki, T. Okuhara, Microporous Mesoporous Mater. 43 (2001) 83.
[22] J.C. Groen, L.A.A. Peffer, J.A. Moulijn, J. Pérez-Ramírez, Colloids Surf. A Physicochem. Eng. Aspects 241 (2004) 53.
[23] J.C. Groen, L.A.A. Peffer, J.A. Moulijn, J. Pérez-Ramírez, Microporous Mesoporous Mater. 69 (2004) 29.
[24] L.L. Su, L. Liu, J.Q. Zhuang, H.X. Wang, Y.G. Li, W.J. Shen, Y. Xu, X.H. Bao, Catal. Lett. 91 (2003) 155.
[25] J.C. Groen, W. Zhu, S. Brouwer, S.J. Huynink, F. Kapteijn, J.A. Moulijn, J. Pérez-Ramírez, J. Am. Chem. Soc. 129 (2007) 355.
[26] J.C. Groen, J.A. Moulijn, J. Pérez-Ramírez, Ind. Eng. Chem. Res. 46 (2007) 4193.
[27] J. Crank, The Mathematics of Diffusion, Oxford Press, London, 1975, p. 203.
[28] H. Thamm, J. Phys. Chem. 91 (1987) 8.
[29] C.K. Lee, A.S.T. Chiang, J. Chem. Soc. Faraday Trans. 92 (1996) 3445.
[30] C.R.A. Catlow, R.A. van Santen, B. Smit, Computer Modeling of Microporous Materials, Elsevier, Amsterdam, 2004, p. 25.
[31] T.J.H. Vlugt, R. Krishna, B. Smit, J. Phys. Chem. B 103 (1999) 1102.
[32] M. Schenk, S. Calero, T.L.M. Maesen, T.J.H. Vlugt, L.L. van Benthem, M.G. Verbeek, B. Schnell, B. Smit, J. Catal. 214 (2003) 88.
[33] A. Corma, Catal. Rev. Sci. Eng. 24 (1982) 1.